Earth and Planetary Science Letters 472 (2017) 174–185

Contents lists available at ScienceDirect

Earth and Planetary Science Letters

www.elsevier.com/locate/epsl

Deformation of mantle pyroxenites provides clues to geodynamic processes in subduction zones: Case study of the Cabo Ortegal Complex, Spain

Hadrien Henry [a,b,*], Romain Tilhac [a,b], William L. Griffin [a], Suzanne Y. O'Reilly [a], Takako Satsukawa [a,c], Mary-Alix Kaczmarek [d,b], Michel Grégoire [a,b], Georges Ceuleneer [b]

[a] Australian Research Council Centre of Excellence for Core to Crust Fluid Systems (CCFS)/GEMOC, Department of Earth and Planetary Sciences, Macquarie University, Sydney NSW 2109, Australia
[b] Géosciences Environnement Toulouse (GET), CNRS, CNES, IRD, Université Toulouse III, 14 avenue E. Belin, 31400 Toulouse, France
[c] Department of Geophysics, Division of Earth and Planetary Sciences, Kyoto University, Kyoto 606-8502, Japan
[d] Institute for Earth Sciences (ISTE), University of Lausanne, UNIL Mouline, Géopolis, 1015 Lausanne, Switzerland

ARTICLE INFO

Article history:
Received 21 February 2017
Received in revised form 13 May 2017
Accepted 16 May 2017
Available online 7 June 2017
Editor: J. Brodholt

Keywords:
mantle pyroxenites microstructure
enstatite
diopside
supra subduction processes
subduction conduit
MTex

ABSTRACT

In the Herbeira massif, Cabo Ortegal Complex, Spain, a well exposed assemblage of deformed dunites and pyroxenites offers a unique opportunity to investigate key upper mantle tectonic processes. Four types of pyroxenites are recognized: clinopyroxenites with enclosed dunitic lenses (*type-1*), massive websterites (*type-2*), foliated and commonly highly amphibolitized clinopyroxenites (*type-3*) and orthopyroxenites (*type-4*). Field and petrological observations together with EBSD analysis provide new insights on the physical behavior of the pyroxenes and their conditions of deformation and reveal the unexpected journey of the Cabo Ortegal pyroxenites.

We show that, during deformation, *type-1* pyroxenites, due to their enclosed dunitic lenses, are more likely to localize the deformation than *types-2* and *-4* pyroxenites and may latter act as preferred pathway for fluid/melt percolation, eventually resulting in *type-3* pyroxenites. All pyroxenite types display a similar response to deformation. Orthopyroxene deformed mostly by dislocation creep; it shows kink bands and undulose extinction and its fabric is dominated by [001](100). Clinopyroxene displays subgrain rotation, dynamic recrystallization and fabric with [010] axes clustering next to the foliation pole and [001] axes clustering next to the lineation suggesting activation of [001]{110} and [001](100) in some samples. These observations are in good agreement with deformation at temperatures greater than 1000 °C. Olivine in *type-1* and *type-4* pyroxenites shows [100](010) or [001](010) fabrics that are consistent with deformation at temperatures >1000 °C and may indicate deformation in a hydrous environment. The amphibole [001](100) fabric gives insights on a lower-temperature deformation episode (~800 to 500 °C). Our results, interpreted in the light of published experimental data, together with the regional geological and geochemical studies are consistent with the following tectonic evolution of the Cabo Ortegal pyroxenites: (1) delamination from an arc root in a mantle-wedge setting at temperatures above 1000 °C and (2) introduction into a relatively softer subduction channel where deformation was accommodated by localized shear zones, thus preserving the high-temperature fabrics of pyroxenites. The Cabo Ortegal pyroxenites may therefore be seen as a rare exposure of deformed mantle-wedge material.

1. Introduction

Rheological models of the upper mantle traditionally adopt a major assumption: the physical properties of mantle peridotites can be satisfactorily inferred from those of olivine. This working hypothesis is being challenged by studies highlighting the potentially important volume of pyroxenes, in the shallow upper mantle and from the transition zone to the crust. Evenly-distributed pyroxenes may modify the bulk rheological properties of peridotites, compared to an unrealistic assemblage of pure olivine, and partly condition their behavior during penetrative deformation. On the other hand, local concentrations of pyroxenes (e.g. layering) may influence the distribution of deformation and lead *inter alia* to

* Corresponding author at: Australian Research Council Centre of Excellence for Core to Crust Fluid Systems (CCFS)/GEMOC, Department of Earth and Planetary Sciences, Macquarie University, Sydney NSW 2109, Australia.
E-mail address: hadrien.henry@mq.edu.au (H. Henry).

http://dx.doi.org/10.1016/j.epsl.2017.05.028
0012-821X/

the nucleation of shear zones. Significant volume of pyroxene-rich lithologies have been reported in many exposures of mantle peridotites (e.g. Dantas et al., 2007; Nicolas and Boudier, 2003; O'Reilly and Griffin, 2013). A growing number of experimental studies (e.g. Amiguet et al., 2010; Bystricky and Mackwell, 2001; Mauler et al., 2000) and studies of natural pyroxene-rich samples (e.g. AvéLallemant, 1978; Frets et al., 2012; Helmstaedt et al., 1972; Muramoto et al., 2011) have addressed the deformation of pyroxenes but more are required to fully understand the processes at work.

The pioneering study of AvéLallemant (1978) was amongst the first to explore the deformation processes in natural websterites and to highlight their complexity. It showed that under high-temperature conditions (i.e. above 1050 °C), the deformation of the volumetrically dominant clinopyroxene (cpx) is mostly accommodated by dislocation creep through non-selective translation gliding, polygonization and syntectonic recrystallization while at lower temperatures, mechanical twining is more common. Similar conclusions were reached by Kirby and Kronenberg (1984) who observed dominance of kink bands and twinning at low temperatures and a switch to subgrain rotation and recrystallization at temperature higher than 1000 °C. Because of the similar lattice shared by omphacite and diopside, studies on eclogites may be extrapolated to understand diopside deformation (Bascou et al., 2002). Omphacite fabrics, characterized by Helmstaedt et al. (1972) and Zhang et al. (2006), which have been shown to give insights on the deformation regime, can therefore be used to understand mantle cpx. The L fabric displays [001] axes clustered next to the lineation and the [010] axes forming a girdle in the plane normal to the lineation; the S fabric is characterized by [010] clustering next to the foliation pole and [001] forming a girdle in the foliation plane and L-S fabric is similar to a [001](010) fabric. These three types of fabrics respectively testify to either shear, axial compression or both. A strong [010] cluster next to the foliation pole was identified as the consequence of slip along {110} planes at high-temperature (>1000 °C) where [001]{110}, and $1/2 < 110 >$ {110} are particularly active (Amiguet et al., 2010; Bascou et al., 2002). Clusters of [100] next to the foliation pole has been reported during axial compression while the $1/2 < 110 >$ {110} duplex is active at high temperatures or at lower temperatures (900 to 1000 °C), when [001](100) slip is activated (Raterron et al., 1994).

Deformation of orthopyroxene (opx) in the upper mantle is less complex because of its simpler crystal structure. In peridotites, high-temperature deformation of opx is typically accommodated by slip along [001](100) forming an AC fabric *sensu stricto* Jung et al. (2010). The appearance of [001](010), was observed in natural specimens as well as in experimental studies, and was suggested to reflect a strain rate greater than 40% (Frets et al., 2012; Mercier and Nicolas, 1975; Nicolas and Christensen, 1987; Ross and Nielsen, 1978).

So far, only few microstructural studies of natural pyroxenites have been carried out. Frets et al. (2012) observed in the Beni Boussera massif that dynamic recrystallization by subgrain rotation, grain-boundary migration and recovery play a major role in the deformation of websterites at high-temperatures (1100–1150 °C and 1.8 GPa). Their observations also suggest that [001]{110} slip in cpx and both [001](100) and [001](010) in opx were activated. Muramoto et al. (2011) studied garnet pyroxenites from the Higashi-akaishi peridotite and showed that [001](100) was dominant at 700–800 °C and 3 GPa with minor activation of [100](010) and $< 110 >$ {110}.

Here we investigate the deformation of pyroxenites from the Herbeira massif of the Cabo Ortegal Complex, Spain, which evolved in a supra-subduction environment (Puelles et al., 2012; Tilhac et al., 2016). We focused on deformed pyroxenite layers exposed in a 300 m-thick pyroxenite-dominated domain (Fig. 1), associated with dunites and harzburgites. Field and microstructural observations are combined with electron backscattered diffraction (EBSD) analyses to characterize the microstructure and the deformation mechanisms involved. Crystallographic data obtained using EBSD are then used to constrain the deformation conditions and relate them to the polyphase tectono-metamorphic evolution recorded regionally.

2. Geological background

The Cabo Ortegal Complex is one of the allochthonous complexes of North-Western Iberia which preserves remnants of the Variscan suture, including ophiolites (e.g. Arenas et al., 1986; Martínez Catalán et al., 2009; Weil et al., 2013). The high-pressure allochthonous units of this complex are mainly composed -of high-pressure gneisses, granulites, eclogites and of granulites and ultramafic rocks (e.g. Albert et al., 2014; Arenas et al., 1986), whose protoliths were probably generated in different parts of the subduction factory (Peucat et al., 1990; Tilhac et al. 2016, 2017). The assembly of these high-pressure units resulted from the combination of subduction and exhumation, notably via subduction-channel processes (Gerya et al., 2002) and orogenic deformations, probably following the closure of the Rheic ocean. This has been accompanied by prograde metamorphism reaching, in the ultramafic units, peak conditions of 1.6–1.8 GPa and 780–900 °C, as recorded by two-pyroxene major-element (Girardeau and Gil Ibarguchi, 1991; Tilhac et al., 2016) and REE thermo(baro)metry (Tilhac et al., 2017). This was followed by retrograde metamorphism under amphibolite- and greenschist-facies conditions (Ábalos et al., 2003 and references therein).

Amongst the three main exposures of ultramafic rocks in the Cabo Ortegal Complex, the Herbeira massif is the largest (~15.5 km^2) and mainly consists of highly serpentinized harzburgites with minor dunites and pyroxenites (Fig. 1). It also preserves relatively fresh and abundant amphibole-bearing pyroxenites interlayered with dunites in a 3 km-long, 300 m-thick zone exposed in the Herbeira cliffs. Spectacular field evidence of high-temperature deformation includes a tectonic foliation parallel to the compositional layering, and boudinage of the pyroxenite layers. Sheath folds (and locally mylonites) were reported by Jamaa (1988) and Tilhac (2017) in the Herbeira massif, and by Puelles et al. (2012) in the Limo massif (Fig. 1) and mostly affect both harzburgites and the pyroxenite-dunite assemblages. They are commonly associated with a higher degree of amphibolitisation.

Measurements of foliations and lineations, despite their strong local variation, lie within the range of previously published orientations of ~N025°/30SE (Ábalos et al., 2003; Girardeau and Gil Ibarguchi, 1991). For simplicity, pyroxenites collected in the Herbeira massif only for this study will be refer to as Cabo Ortegal pyroxenites.

3. Material and methods

3.1. Sample selection

A set of 16 oriented samples was selected, 10 from the pyroxenite-rich area and 6 scattered around the massif (Fig. 1). Due to their very high degree of serpentinization leaving only a meager proportion of olivine grains, dunites and harzburgites were not included in this study. Pyroxenites were less affected by low-temperature alteration and thus offer excellent material for textural and EBSD studies. The chosen samples are representative of Cabo Ortegal pyroxenites following the petrological systematics defined by Tilhac (2017) and Tilhac et al. (2016) who identified four lithological types. *Type-1* groups olivine-clinopyroxenites and websterites including dunitic lenses observable at both outcrop- and thin-section scales (Fig. 2A and D). Massive olivine-free web-

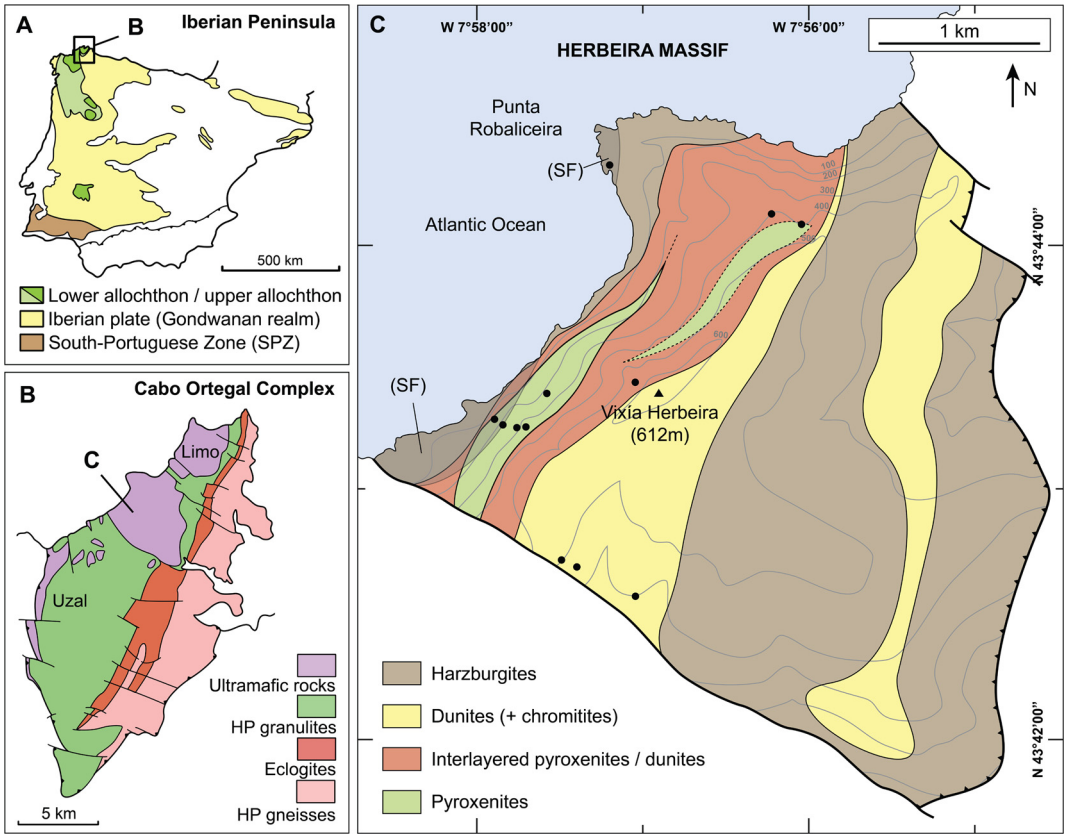

Fig. 1. (A): location of the Cabo Ortegal Complex on the Iberian Peninsula (after Puelles et al., 2012); (B): simplified map of the high-pressure units of the Upper Allochthon (after Llana-Fúnez et al., 2004); C: geological map of the Herbeira massif (modified after Tilhac et al., 2016). SF indicates the areas where sheath folds have been observed. Sample locations are indicated by the black dots. The black triangle indicates the Herbeira massif highest point. Outline of the eastern dunite body after Puelles et al. (2012).

sterites (i.e. with higher opx/cpx ratios) and commonly devoid of dunite lenses are classified as *type-2* pyroxenites (Fig. 2B and E), while *type-3* pyroxenites consists of foliated clinopyroxenite and few websterites, commonly strongly amphibolitized (Fig. 2C and F). *Type-4* pyroxenites represent uncommon orthopyroxene-rich websterites and orthopyroxenites.

3.2. Analytical procedures

Thin sections were cut in the structural XZ plane (*cf.* Fig. 4) to allow the determination of fabrics. A colloidal silica–water solution (mixed in 70/30 proportion) was used at the final stage of polishing for 5 min to reduce surface damage produced by mechanical polishing. Crystallographic orientations of minerals were acquired using a HKL NordlysNano electron backscatter diffraction(EBSD) detector attached to a Zeiss EVO MA15 scanning electron microscope (SEM) in the Geochemical Analytical Unit (GAU) at GEMOC/CCFS, Macquarie University, Australia. Kukichi bands were obtained by the interaction between the sample tilted at 70° and the incoming electron beam. For all analyses, a 15 µm step size was used. The working distance varied between 15 and 20 mm depending on the sample and the analysis location within the sample. Automatic indexing was performed using the AZtec software (Oxford Instruments). The HKL software was used to perform a standard noise reduction and to extrapolate the missing data with at least 8, 7, 6 and then 5 identical neighbors with similar orientation. Resulting EBSD data were then processed using MTex (Bachmann et al., 2010, 2011). The processing protocol included: (1) removing measurements with a mean angular deviation greater than 1.3; (2) defining grains by enforcing that any two neighboring measurements belong to the same grain if their orientation difference is less than a specific threshold. We used a 10° threshold; this is the value classically used in Earth Sciences, and allow accurate comparison of the results with previous studies; (3) smoothing and interpolating the missing data within the grains, and (4) removing grains with a surface smaller than 10 pixels to avoid bias caused by potential indexing error.

To avoid oversampling of large grains, and allow fabrics comparison between samples, pole figures with one point per grain were plotted on a lower-hemisphere, equal-area stereographic projection. When the number of grains is higher than 100, orientation density functions (ODF) have been calculated with a 10° Gaussian half-width. The ODF strength of each crystallographic axis was estimated using the J-index (Bunge, 1982). The strength of the crystallographic preferred orientation (CPO) was estimated using both the J-index and the M-index (Bunge, 1982; Skemer et al., 2005). For all pole figures, contours have been plotted at each multiple of the uniform distribution to allow for a clearer and an easier comparison between the samples. The Matlab scripts used to produce the figures as well as all the fabrics are provided in the Electronic Appendices (Electronic appendices 3–8). The misorientation of each pixel was calculated relative to the mean orientation of its corresponding grain, and then combined as maps of "misorientation relative to mean grain orientation". Any misorientation value greater than 10° was brought down to 10° to allow for a clearer observation.

4. Results

4.1. Texture and microstructure

A detailed description of the texture, microstructure and chemical composition of the different types of pyroxenite has been provided by Tilhac et al. (2016) and Tilhac (2017) where further

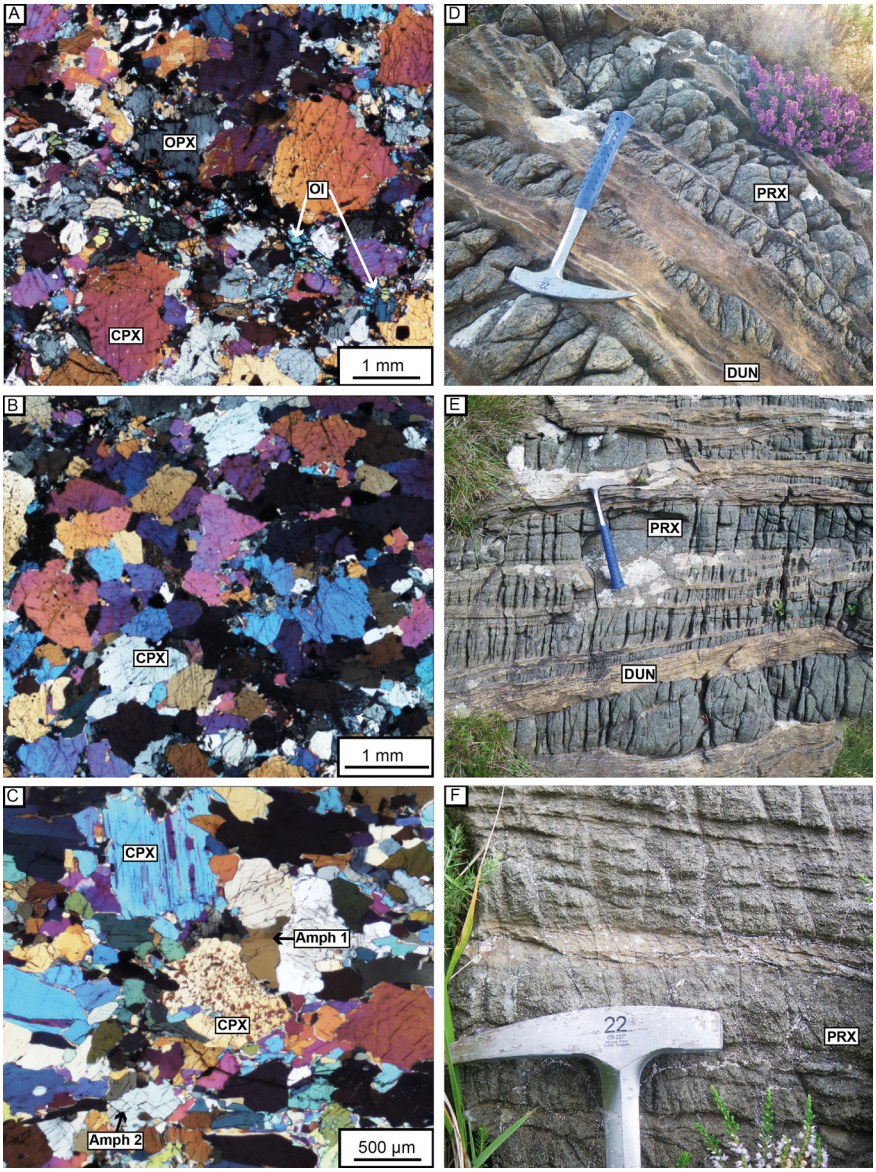

Fig. 2. Photomicrograph illustrating (A) the dominant porphyroclastic texture in a *type-1 pyroxenite* (sample CO-096-A/B), (B): an equigranular texture in sample 701BA; (C): two textural relationships between amphibole and pyroxenes in a *type-3* pyroxenite with xenomorphic (Amph 1) and idiomorphic to sub-idiomorphic (Amph 2) grains. Field photographs illustrating the occurrence of (D) *type-1* pyroxenites, with interstitial dunite (note the boudinage of the pyroxenite layers), (E) *type-2* massive pyroxenites with massive appearance and (F) *type-3* pyroxenites, exhibiting a characteristic thinly foliated aspect.

details can be found. For simplicity, we present here a concise description of the microstructure of the four types of pyroxenites as well as a description of the dominant phases forming the Cabo Ortegal pyroxenites: opx, cpx, olivine and amphibole. Because (1) this study is focused on the pyroxenites and (2) the impossibility to analyse minerals with very different strength on a single thin section with EBSD, phases such as spinel and sulfide, or minerals related to low-temperature alteration, such as serpentine, were not studied at all here. Garnet also was not considered here as it is present in only a few samples.

Type-1 pyroxenites (clinopyroxene-rich websterites and clinopyroxenites, Figs. 2A and 2D) have a dominantly porphyroclastic texture, except for sample 701BA which displays an equigranular texture (Fig. 2B). The grain-size distribution is thus bimodal and large grains make up ~50% of the rock volume. In *type-1* pyroxenites, cpx makes up most of the surface area. It is associated with amphibole, which represents on average 10% of the surface area; olivine (and less commonly opx) may also be present in similar proportions.

In *type-2* pyroxenites (olivine-free websterites, Fig. 2E) the modal abundance of opx is higher than in *type-1* pyroxenites (20 to 30% of surface area); olivine is absent and amphibole makes up ~20% of the surface area (Figs. 5B and 5C). The grain size distribution in *type-2* is similar to that in *type-1* pyroxenites. Coarse cpx and opx grains make up 55% of the rock volume. The texture is mostly porphyroclastic and the grain boundaries of porphyroclasts indicate the absence of textural equilibrium between pyroxenes, either due to dynamic recrystallization or to the presence of amphibole neoblasts.

Type-3 pyroxenites (foliated clinopyroxenites and websterites, Fig. 2F) are strongly amphibolitized (up to 55% of the surface volume) and locally becomes a quasi-bimineralic assemblage of cpx and amphibole (Fig. 2C). Levels of large and unstrained grains of amphibole can be observed parallel to the tectonic foliation (Electronic Appendix 2B). In contrast to *type-1* and *-2* pyroxenites, the grains-size is dominantly equigranular with a grains equivalent diameter of ~800 µm. Such a grain size distribution probably results of the growth and/or the static recrystallization of amphibole along

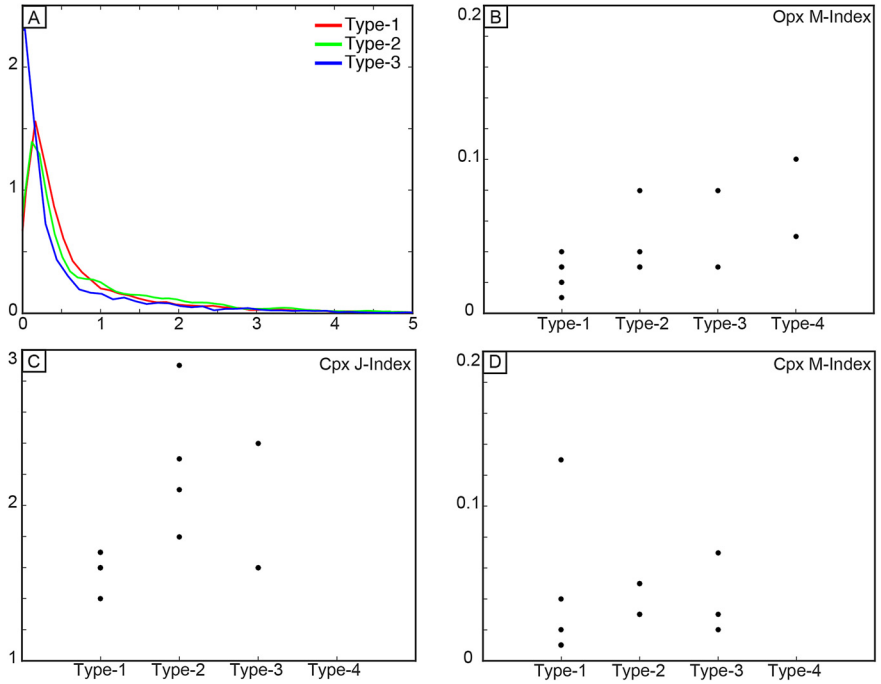

Fig. 3. Trends observed in the CPO data from Cabo Ortegal pyroxenites. (A) Probability-density function of the Grain Orientation Scattering (GOS) in degree for all cpx grains in *type-1*, *-2* and *-3* pyroxenites (i.e. the average deviation in orientation between each point in a grain and the mean grain orientation). While the distinction between *type-1* and *type-2* is subtle, indicating a similar level of internal deformation, *type-3* pyroxenites clearly have more equilibrated cpx than the other two types; (B) and (D): M-index of opx and cpx CPO for each type of pyroxenite; (C) J-index of cpx for each type of pyroxenite. Sample 701BA has been excluded from the plots because of its anomalously high J and M indexes compared to the other *type-1* pyroxenites.

pyroxenes grain boundaries and among matrix minerals, as described by Tilhac et al. (2016) and Tilhac (2017).

Type-4 pyroxenites (opx-rich websterites and orthopyroxenites) contains more than 70% of opx. The modal proportion of olivine ranges from 5% to 20% in some samples, amphibole occurs in a proportion similar to that in *type-1* pyroxenites and rare cpx may be observed. The grain-size distribution is also bimodal but is here dominated by porphyroclasts; opx accounts for the coarse fraction while opx, cpx and/or amphibole constitute the fine-grained one.

In all the types of pyroxenites, opx (enstatite) may be observed as porphyroclasts (500 µm up to 3 mm) displaying undulose extinction and kink bands highlighted by exsolved spinel and/or cpx (Fig. 5C). Grain boundaries are complex, irregular and shaped by various equilibrated neoblasts (∼ 175 µm) grown at the expense of the unrecovered porphyroclasts and accounting for a smaller proportion of the surface area (Fig. 7B). Similarly, cpx (diopside) occurs as porphyroclasts hosting exsolved spinel along cleavage and exhibit a range of grain size similar to that of opx. It also displays complex and irregular grain boundaries. Subgrain boundaries near the contacts with surrounding grains, and sometimes undulose extinction, can be observed in most grains. Cpx also occurs as misorientation-free neoblasts comparable in size to the opx neoblasts (Figs. 4B and 6A). Olivine (forsterite 0.86–0.89) may occur as relics of larger grains that have been serpentinized (i.e. mesh texture) forming bands in *type-1* pyroxenites, as inclusions in pyroxenes but most commonly as elongated and recovered interstitial grains in *type-1* and *-4* pyroxenites (Electronic Appendix 2B). Their grain size is relatively homogeneous with a mean equivalent diameters of the grain of ∼160 µm.

Amphibole (magnesiohornblende) is observed in all samples as lamellae, replacing exsolved cpx and/or locally associated with spinel opx and cpx or as interstitial grains between the pyroxenes, resulting in sutured grain boundaries of cpx porphyroclasts. When occurring within pyroxenes, idiomorphic to sub-idiomorphic grains occur preferentially along the pyroxenes cleavage can be observed. These observations suggest that some of the amphibole have grown at the expense of clinopyroxene (Figs. 2C, 6 and Electronic Appendix 2C and D). The growth of amphibole depending on its modal abundance and on the type of pyroxenite, has resulted in various textural overprints, notably responsible for the co-existence of porphyroclasts in otherwise equigranular samples. Based on grain shape and the internal deformation, two populations of amphibole grains can be distinguished: (1) idiomorphic to sub-idiomorphic grains (Amph 1 in Fig. 2C and Electronic Appendix 2), with no sign of internal deformation; (2) xenomorphic grains (Amph 2 in Fig. 2C) with a higher degree of lattice misorientation, in the form of undulose extinction or subgrain boundaries, especially in grains squeezed between two pyroxene grains. These grains are xenomorphic and have more irregular boundaries. Both populations have comparable major and trace-element composition within a given sample (Tilhac et al., 2016) and may cover the whole range of the amphibole grain size, which has a mean value of ∼180 µm (see Electronic Appendix 1).

Our field data and petrographic observations do not allow us to define any relationship between the pyroxenes deformation markers, the different types of pyroxenite, their location and the thickness of the layer. On the contrary, and with the exception of sheath folded area, any macro- or micro-scale deformation marker and textures can be found anywhere in the massif.

4.2. Fabrics and internal deformation from EBSD

EBSD analysis of intracrystalline deformation in *type-1* pyroxenites reveals a relatively low degree of lattice misorientation (Fig. 4B). Rare concentrations of misorientations occur in the tips of large cpx grains at contacts with other cpx porphyroclasts and along subgrain. With the exception of sample 701BA, both M and J indices are low (0.01 for M and 1.6 for J-index; Electronic Appendix 1), indicating a rather weak CPO for cpx. CPO also suggests weak cpx fabrics but a [001](010) pattern (SL fabric) is nevertheless observable in half of the samples (Electronic Appendices 1 and 3). Either a random distribution or the presence of [001](100)

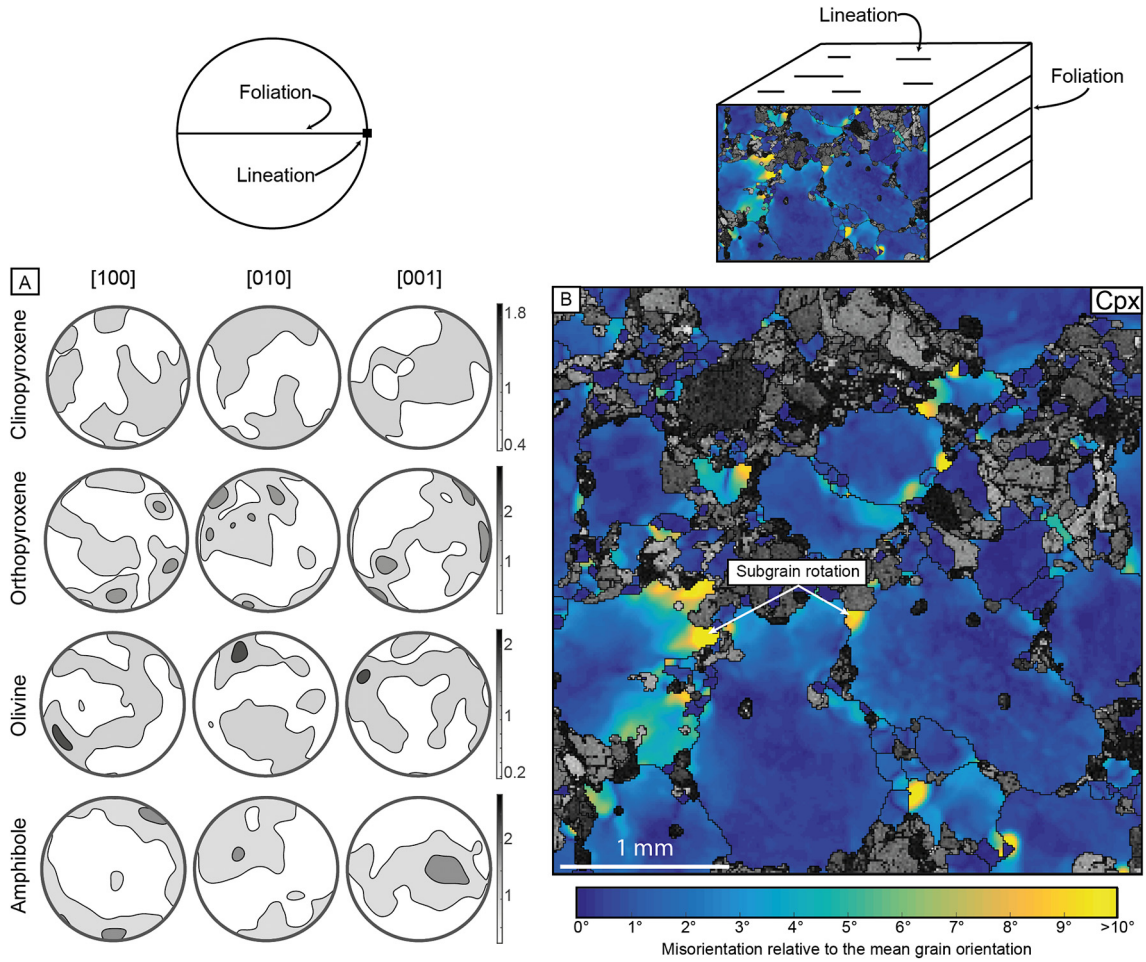

Fig. 4. (A) CPO of cpx, opx, olivine and amphibole and (B) color-coded EBSD map of a *type-1* pyroxenite (CO-096-A/B) showing for cpx the misorientation to the mean grain orientation for each measurement (i.e. pixel). Yellow color indicates a deviation of 10° or more from the mean grain orientation while dark blue indicates a value close to the mean grain orientation. (For interpretation of the references to color in this figure legend, the reader is referred to the web version of this article.)

as in the case of sample CO-096-A/A makes up for the other half of the samples. Rare opx grains may define either a weak [001](100) fabric or a random distribution (Fig. 4A). Olivine CPO is weak and mostly random but still allows the determination of [001](010) fabric in 3 samples and of [100](010) fabric in another one (Fig. 4A). A [001](100) fabric of amphibole seems to dominate in *type-1* pyroxenites (Fig. 4A). This fabric is consistently stronger than the fabrics of pyroxenes and olivine (0.05 for M and 2.7 for J-index) and may display a point maximum, girdles or a random distribution depending on the sample and the axis considered. Beside [001](100), amphibole from sample 401A (Fig. 8) and 100B display a [010](100) fabric and [001](010) is found in sample CO-96-A/B and 702A.

Optically, the intracrystalline deformation recorded in *type-2* pyroxenites (olivine-free massive websterites) appears stronger than in *type-1* pyroxenites (Fig. 5). However, a probability-density function of the grain orientation spread (GOS) of the volumetrically dominant cpx reveals that the two types are very similar from an internal-deformation point of view (Fig. 3A). In *type-2* pyroxenites, cpx fabrics are dominated by [001](010) (i.e. SL-type fabric) except for sample CO-099-A which displays a S-type fabric. Opx has a very homogeneous [001](100) fabric. Although the M and J indexes of pyroxenes are slightly greater than in *type-1* pyroxenites (Fig. 3C and D), our data do not allow us to propose a viable statistical interpretation because of the limited number of samples. Amphibole fabrics display the same variability as observed in *type-1* pyroxenite with [001](100), [001](010) or even (010) with two girdles formed by [100] and [001] axes (Fig. 5A, Electronic Appendices 1 and 4).

In *type-3* pyroxenites, the internal energy seems optically similar to that of *type-1* (i.e. misorientations restricted to grain and subgrain boundaries; *cf.* Fig. 6), but this is mainly due to the lack or the low abundance of opx. Subgrain rotation can be observed in large cpx grains and strong lattice misorientations may appear in some amphibole grains (Fig. 6B). Cpx fabrics are [001](010) and can be both of S or L-type. Thanks to the high modal abundance of amphibole, the two different populations described above are here easily visible. Amphibole shows a striking [001](100) fabric with, in sample CO-067-B, a girdle formed by [100] along the plane normal to the lineation. Large idiomorphic amphiboles with shapes matching the foliation and lineation reference frame can be observed in sample CO-067-A (Electronic Appendix 2A).

In *type-4* pyroxenites, internal deformation is particularly striking. Kink bands are abundant and their axes are sub-normal to normal relative to the main foliation (Fig. 7B). Finer grains (of all phases) are well-equilibrated internally compared to the large porphyroclasts, and only rarely display evidence of misorientation. Opx displays a strong [001](100) fabric which also occurs in amphibole with a notably strong linear component (Fig. 7A). The combination of [100](010) and [001](010) fabrics for olivine is suggested in sample 704A. Due to the limited number of grains (i.e. $<$100 grains), the contours of the cpx ODF have not been drawn and the J and M index excluded. However, both selected *type-4* pyroxenites show a strong concentration of the three cpx crystal-

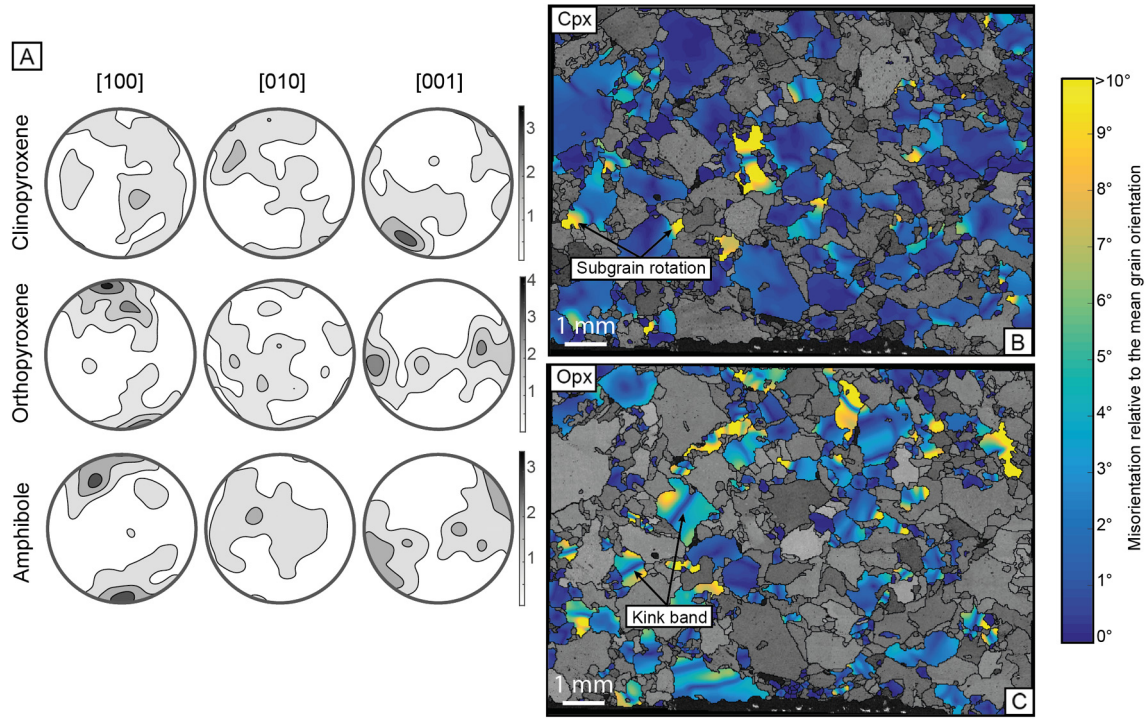

Fig. 5. (A) CPO of cpx, opx and amphibole of a *type-2* pyroxenite (CO-097-A); (B) and (C) show the misorientation to the mean grain orientation for cpx and opx in the same sample respectively. Note the difference in microstructure and deformation behavior between opx and cpx. (For an accurate understanding of the figure, the reader is referred to the web version of this article.)

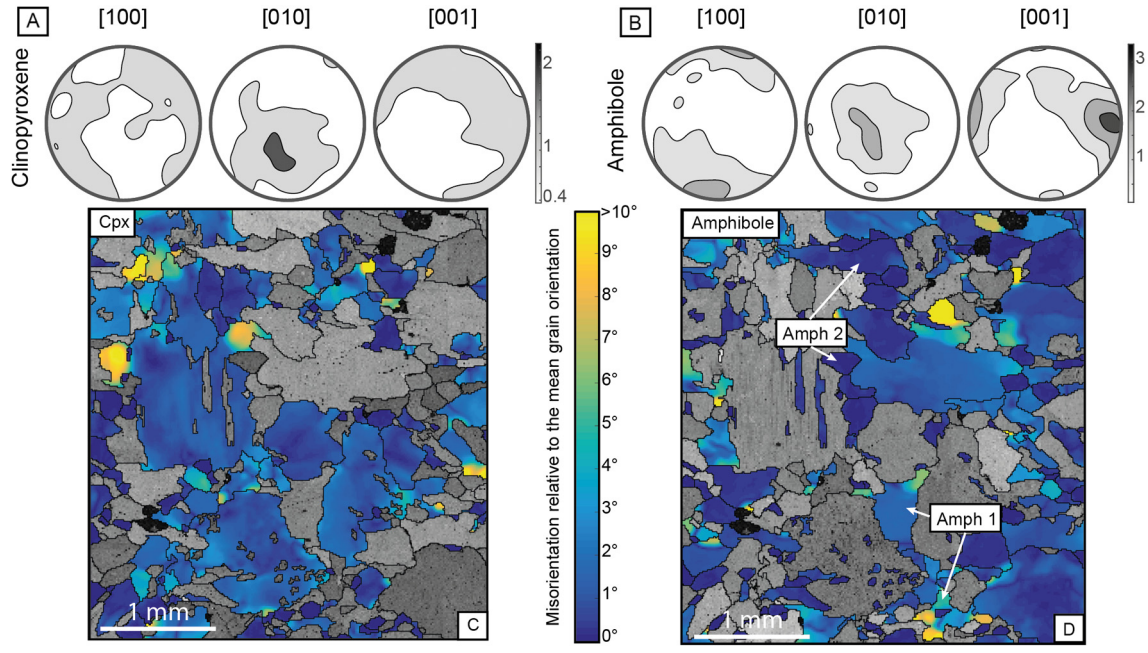

Fig. 6. CPO and color-colored EBSD map of a *type-3* pyroxenite (CO-101-C) showing the misorientation of each measurement to the mean grain orientation for (A) cpx and (B) amphibole. Idiomorphic (Amph 2) and xenomorphic (Amph 1) grains are clearly visible here. (For an accurate understanding of the figure, the reader is referred to the web version of this article.)

lographic axes modulo a 90-degrees' rotation around the [100] axis (Fig. 7).

5. Discussion

5.1. Conditions of deformation of the Cabo Ortegal pyroxenites

In this section, the significance of the fabrics of the four main rock-forming minerals is discussed and the possible deformation regimes and temperatures are inferred.

The average grain size of cpx neoblasts computed from ESBD data (Electronic Appendix 1) was used to estimate the differential stress following the relation of AvéLallemant (1978). Results are relatively homogeneous, exhibiting a mean value of 30.8 ± 7.6 MPa (Electronic Appendix 1). Sample 401A, which represents the contact between a pyroxenite layer and its host dunite, displays a much higher differential stress of 101 MPa. The [001](010) fabric in cpx is visible in most samples and does not seem to be correlated with a specific type of pyroxenite. Such fabric, possibly related to

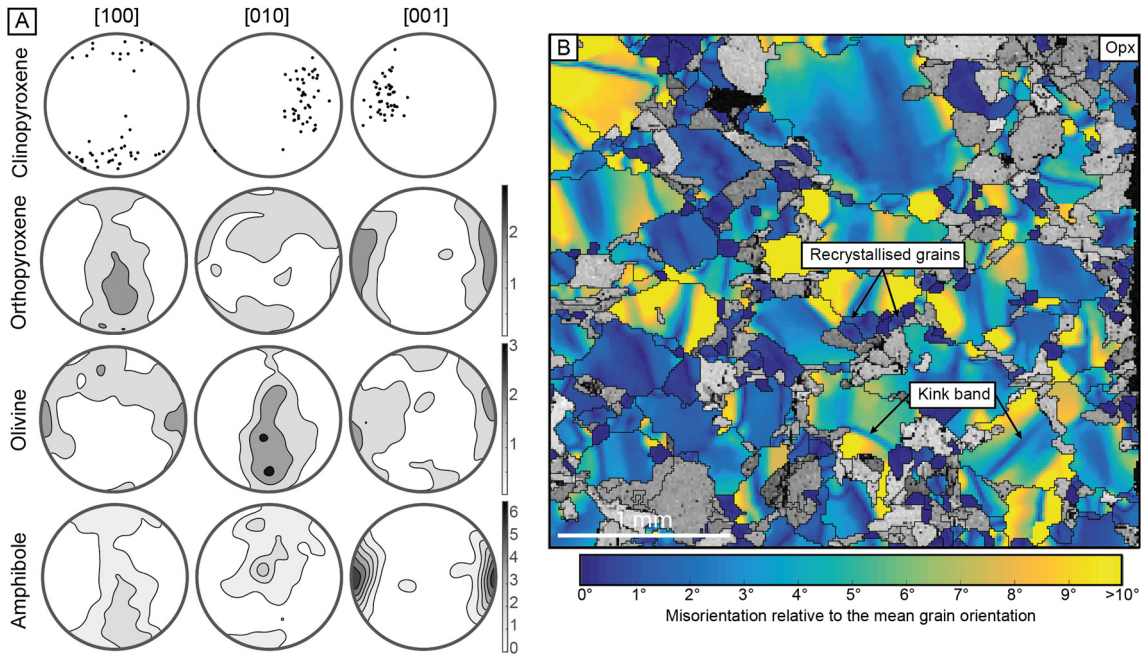

Fig. 7. (A) CPO of cpx, opx, olivine and amphibole and (B) color-coded EBSD map of *type-4* pyroxenite (704A) showing for opx the misorientation of each measurement to the mean grain orientation map. (For an accurate understanding of the figure, the reader is referred to the web version of this article.)

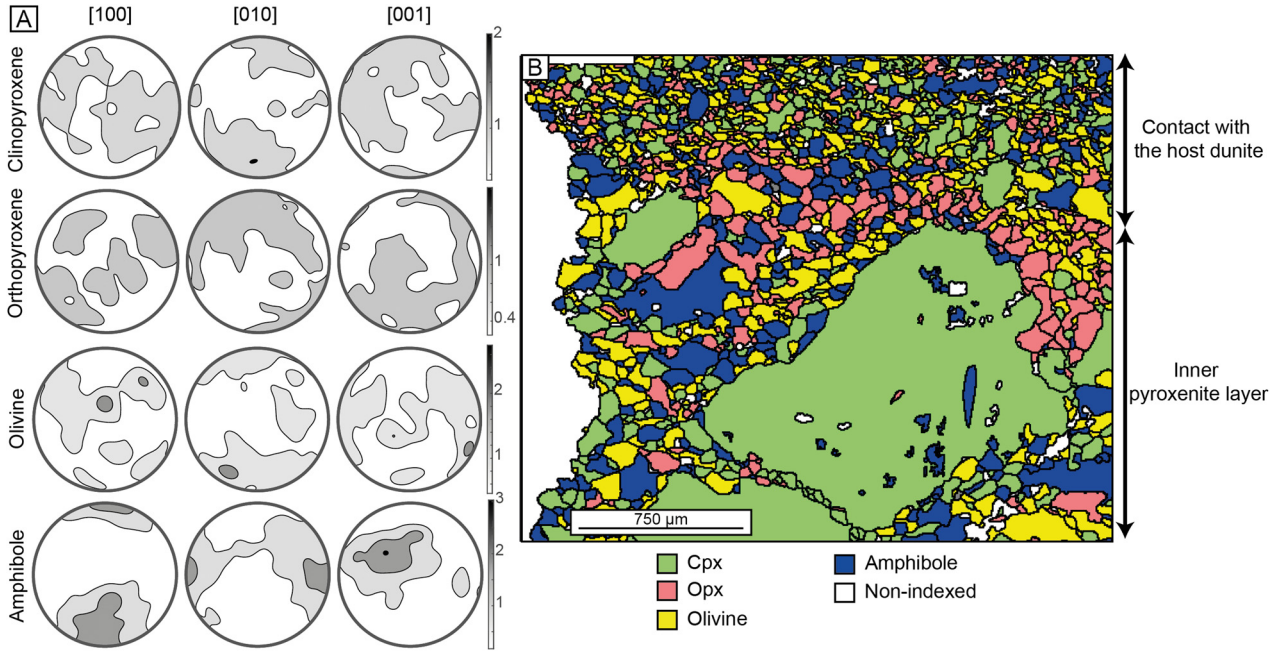

Fig. 8. (A) CPO of cpx, opx, olivine and amphibole in a *type-1* pyroxenite (sample 401A) and phase map (B) of the same sample at the contact between host dunite and pyroxenite, where grain size reduction occurs. Note the amphibole fabric differing from the commonly observed [001](100) and the rather weak fabrics of the pyroxenes and olivine.

slip along [001]{110} and $1/2 < 110 > \{110\}$, was described as the main deformation mechanism at temperatures >1000 °C (Amiguet et al., 2010; Bascou et al., 2002). Additional clustering of [100] axes next to the foliation pole on top of the [001](010) fabric observed in samples CO-096-A/A, 706AA and CO-097-A/A (Electronic Appendices 3 and 4) may indicate the activation of [001](100) and/or the relative domination of $1/2 < 110 > \{110\}$ (Amiguet et al., 2010; Raterron et al., 1994). Considering that the formation of the [100] cluster by $1/2 < 110 > \{110\}$ would require an axial compression at high-temperature, one would expect an S-type fabric in these cases, which is not observed. The activation of [001](100) at lower temperature (900 to 1000 °C) is therefore more consistent with our observations and could explain the [100] clustering next to the foliation pole. This clustering of cpx [100] axis next to the foliation pole in *type-4* pyroxenites may be regarded as an evidence for the latter deformation, although it could alternatively be interpreted as reflecting an effect of modal composition on the cpx fabric. Besides, considering that no mechanical twins or kinks were observed, clinopyroxene did not record deformation at lower temperatures (i.e. <900 °C). S-, L- and SL-type fabrics being unrelated to the different types of pyroxenite, we propose that deformation regimes may essentially reflect the initial orientation of the pyroxenite layers/dykes relative to the paleo-stress field.

Based on these results, we suggest that cpx in Cabo Ortegal pyroxenites recorded deformation at temperatures greater than 900 °C, and mostly higher than 1000 °C. This high-temperature deformation event included either a shear component, an axial compression component or both depending on the sample.

The grain size of opx neoblasts has been used to estimate the differential stress following the relation of Ross and Nielsen (1978). It shows consistent results with that observed in cpx yielding a mean value of 20.3 ± 5.1 MPa. Again, sample 401A records a greater differential than the others samples with an estimated stress of 103 MPa. In most pyroxenites and in all types of pyroxenites, opx fabrics seem to indicate the activation of [001](100) glide (i.e. AC-type fabric of Jung et al., 2010) which has been widely reported in upper mantle samples (Nicolas and Christensen, 1987). In contrast to the results of Jung et al. (2010), we observe an increasing CPO strength with increasing opx content and a [001](100) fabric regardless of the modal proportions (Electronic Appendix 1). Assuming a water-rich environment and a strain rate of 10^{-13} s^{-1} (Ábalos et al., 1996, 2003; Puelles et al., 2009; Tilhac et al., 2016), deformation by transformation to clino-enstatite can be estimated to occur below ∼800 °C (Ross and Nielsen, 1978). The absence of observed clino-enstatite may thus suggest that opx recorded deformation at temperatures greater than 800 °C. However, although the occurrence of clino-enstatite has never been reported in the Cabo Ortegal pyroxenites, its presence cannot be ruled out altogether and a more conservative interpretation has to be retained.

Even if the opx fabric, kink band and undulose extinction are consistent with deformation at mantle conditions, we will consider the opx to be inconclusive when it comes to defining a temperature field for that deformation event.

The A- and B-type olivine fabrics observed in *type-1* and *type-4* pyroxenites suggest the activation and of [100](010) and [001](010) slips respectively. The A-type fabric is commonly found in upper-mantle peridotites and has been observed in high-temperature, low-stress environments in a wide variety of xenoliths (Ismaïl and Mainprice, 1998; Nicolas and Christensen, 1987). B-type fabric is produced (1) during the A- to B-type transition upon a decrease in temperature and/or an increase in stress (Carter and Ave Lallemant, 1970); (2) at high-temperature upon an increase in the olivine water content and a possible increase of stress (Jung and Karato, 2001); (3) at pressure greater than 3 GPa in a dry environment (e.g. Jung et al., 2009; Ohuchi et al., 2011); (4) between 5 and 8 GPa with a relatively low proportion of opx (Soustelle and Manthilake, 2017). In the Cabo Ortegal Complex, the peak metamorphism reached a pressure of ∼1.7 GPa, excluding the possibility of a pressure triggered B-type fabric. The heterogeneous distribution of the phases (i.e. the layering), the lack of cpx and the different pressure ranges at which the experiments were carried out makes it difficult to use the results of Soustelle and Manthilake (2017) to understand the fabrics of the Cabo Ortegal pyroxenites. Consequently, the origin of B-type fabrics in the Cabo Ortegal pyroxenites is likely to be the result of variations in stress, temperature and/or water content. B-type fabrics have been documented in the harzburgites of the neighboring Limo massif (Puelles et al., 2012) and were interpreted as a result of decreasing temperature and an increasing stress. In the Cabo Ortegal pyroxenites, formation of a B-type fabric by a stress-induced transition from A to B is not consistent with our differential stress calculations: while the B-type fabric is found in the most stressed sample (i.e. sample 401A), it is also found in other samples exhibiting the same range of stress as A-type fabric (Electronic Appendix 1). The lack of lattice misorientation in the olivine grains of the Cabo Ortegal pyroxenites also suggests a re-equilibration of the lattice (Electronic Appendix 2-B) at sufficient temperatures for efficient diffusion to operate. This thus excludes a simple temperature decrease as a cause of the B-type fabric.

We conclude that the olivine found in Cabo Ortegal pyroxenites recorded deformation at temperatures greater than 1000 °C and most likely testifies to a hydrous environment.

Among the main rock-forming phases in the Cabo Ortegal pyroxenites, amphibole has the strongest fabric, with [001](100) appearing in most samples (*cf.* Figs. 4A, 5A, 6A and Electronic Appendix 1). This fabric has been observed in deformation experiments and natural sample at temperatures between ∼500 °C and 800 °C (Dollinger and Blacic, 1975; Getsinger and Hirth, 2014; Ko and Jung, 2015). Along the contacts between pyroxenite and dunite (i.e. sample 401A), a fabric switch to [010](100) is observed (Fig. 8). This switch in fabric has also been observed experimentally and was linked to a potential increase in stress (Ko and Jung, 2015). Amphibole CPOs display values of mean uniform distribution that could be interpreted as the result of a cataclastic process (Díaz Aspiroz et al., 2007). However, such interpretations are not consistent with the textural and petrographic observations on the Cabo Ortegal pyroxenites, suggesting that only little deformation was recorded by the most amphiboles. As noted before, amphibole is the phase with the strongest fabrics in the Cabo Ortegal pyroxenites. We interpret the greater strength of amphibole fabrics relative to the one of pyroxenes and olivine as the result of an oriented growth taking place in a stronger stress field than the one that is related to the pyroxenes and olivine fabrics. The mimicking of cpx CPO by amphibole, which is observed in some of our samples, indicates that some proportion of the amphiboles has grown after cpx and inherited its crystal orientation. This is consistent with the close textural relationships shared by amphibole and cpx (Tilhac, 2017; Tilhac et al., 2016), their relative isotopic equilibrium (Tilhac et al., 2017) and similar observations made in the Limo massif (Puelles et al., 2012), supporting the idea of a metamorphic origin for at least part of the amphibole grains. The alignment of amphibole fabrics with the structural framework and its abundance in Cabo Ortegal pyroxenites suggest that the lineation observed at macroscopic scale is mostly defined by amphibole grains. Only in *type-4* pyroxenite, which is relatively poorer in amphibole, the lineation is dominated by elongated and well-aligned opx grains.

On the basis of the textural observations and fabrics, we conclude that amphibole recorded mainly a low stress plastic deformation at a temperature ranging from ∼800 to a minimum of 500 °C, after the higher temperatures episode recorded by the pyroxenes and olivine.

Mineral fabrics in the Cabo Ortegal pyroxenites reveal two distinct deformation events: opx, cpx and olivine testify to deformation at high temperatures and low stress compatible with an upper mantle setting (>1000 °C), possibly in a hydrated environment, while amphibole recorded a lower-temperature deformation (∼800 down to a minimum of 500 °C) probably mainly accommodated by strongly serpentinized harzburgitic or dunitic host. Our results also indicate that Cabo Ortegal pyroxenites were deformed under relatively low-stress conditions during both episodes. The consistency of opx [001](100) and cpx [001](010) fabrics and their close spatial coincidence suggest that all Cabo Ortegal pyroxenites recorded the same high-temperature deformation overprinting any previous microstructural differences acquired previously.

5.2. Lithological constraints on the development of microstructures

Aside from the fabrics, the degree of internal deformation for each type of pyroxenite is here quantified in order to assess the lithological constraints imposed on the development of microstructures. For that purpose, we have calculated GOS probability-density functions for the volumetrically dominant cpx (Fig. 3a). Results suggest that cpx in both *type-1* and *-2* pyroxenites show quite relatively similar internal deformation. Therefore, any subjective

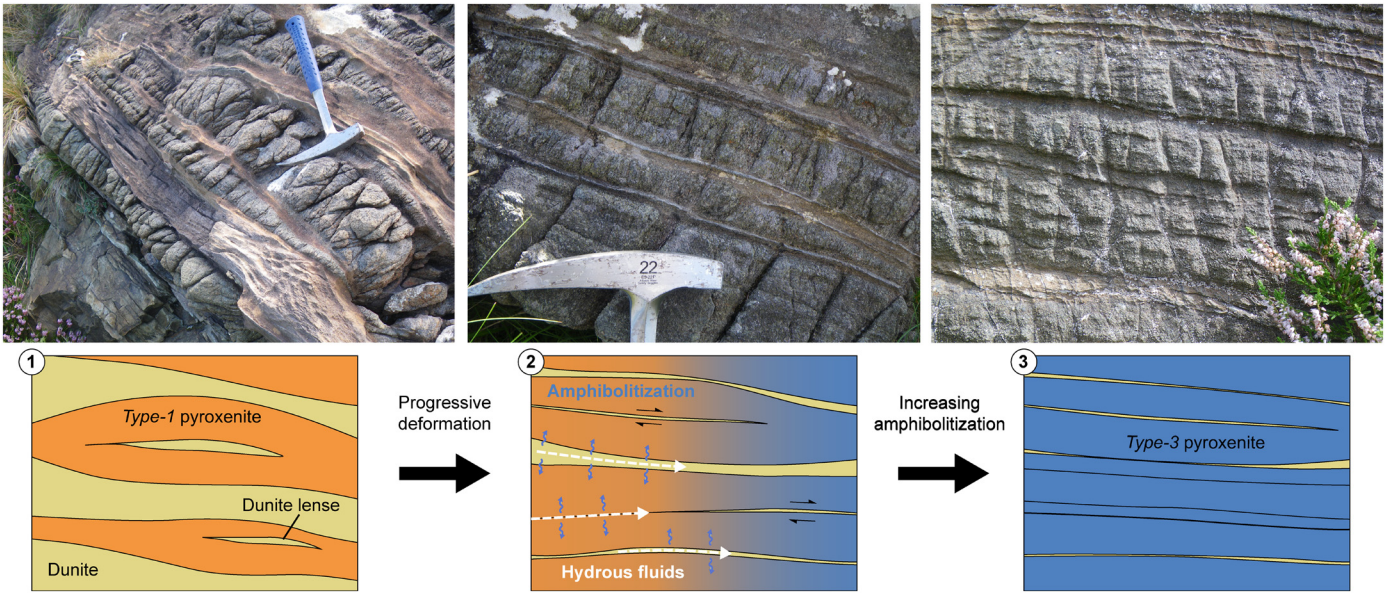

Fig. 9. Sketch depicting the model proposed by Tilhac (2017) for the formation of *type-3* pyroxenites from on a protolith similar to those of *type-1* pyroxenites; increasing deformation by axial compression and shear eventually stacks pyroxenites layers (1 and 2) creating preferential pathways for fluid percolation and amphibolitization (3).

estimate of a deformation difference in thin section is likely to be the result of the modal composition and notably the higher abundance of opx, best illustrated in *type-4* pyroxenites. However, the cpx GOS of *type-3* pyroxenites is different from the other types and indicating a generally lower internal energy consistent with petrographic observations.

As described above, EBSD maps and petrographic observations consistently indicate two populations of amphibole grains: one of idiomorphic and unstrained grains (Amph 1, Fig. 2F) and another of xenomorphic and un-equilibrated grains (Amph 2 in Fig. 2C, *cf.* Fig. 6B and Electronic Appendix 2). EBSD data allow the estimation of the mean surface area for each population. Using a petrographically realistic GOS threshold of 2 degrees to separate the two populations, one can estimate that ~20% of the amphibole volume in the Cabo Ortegal pyroxenites is represented by xenomorphic amphibole. This value being roughly constant regardless of the pyroxenite type and therefore it excludes the possibility of using amphibole deformation as a criterion to differentiate between the pyroxenite types. Nonetheless, it can be interpreted as an evidence for a mostly post-kinematic amphibolitisation.

In previous works, Tilhac et al. (2016) suggested, based on the low modal proportion of opx and their foliated aspect outlined by dunitic levels, that *type-3* pyroxenites may represent the deformation product of a protolith similar to the one that formed *type-1* pyroxenites (Fig. 9). Such a process would have several consequences for the microstructures and can be tested. One would require the pyroxenites to be mechanically stronger than the host dunite so that the deformation would be localized in the dunitic lenses. As observed in sample 401A, grain size reduction and the relatively high-stress amphibole fabric suggest that the deformation is mainly accommodated by the host rock. In addition, flow laws for deformation of websterites and dunites in a hydrated environment under upper mantle conditions (0.5 to 1.5 GPa of confining pressure) predict a high viscosity contrast, between websterites and dunites, which would tend to localize the deformation in the dunites (AvéLallemant, 1978). Accordingly, the deformation mechanism needed to produce the lamination of the dunitic lenses in *type-1* pyroxenites is evidenced by the S- and SL-cpx fabrics in the pyroxenites. A corollary of this process, and especially of the grain size reduction is preferential paths for subsequent fluid/melt percolation. The lower GOS in *type-3* pyroxenites cpx which may be interpreted as the result of a lattice re-equilibration in the presence of a fluid, and the high abundance of amphibole are both compatible with this process.

Our results show that the internal deformation of minerals allows to distinguish between *type-1* and *-2* pyroxenites together from *type-3* pyroxenites, *type-4* pyroxenites being essentially distinctive due to their modal composition. Microstructural features are especially consistent with a process that may produce Cabo Ortegal *type-3* pyroxenites from the deformation and hydration of a similar protolith as the one of *type-1* pyroxenites. The implications of this are two-fold and potentially have a global significance for the evolution of mantle domains: (1) during deformation, replacive pyroxenites such as the Cabo Ortegal *type-1* pyroxenites may represents preferential location for fluid and shear zones development; (2) as a corollary, their presence in recycled mantle domains is likely to be commonly obscured (and thus underestimated) because of the overprint of metasomatic reactions and thus the formation of deformed pyroxenites and hornblendites. A similar process, where deformation controls pyroxenite formation, was suggested by Chen et al. (2001) based on xenolith studies. By bringing statistical quantification of the mineral deformation via the GOS and mineral fabrics, the present study is thus the first to provide robust microstructural evidence to support this hypothesis.

5.3. Tectonic and geodynamic implications

In the field, both isoclinal folds, which indicate of a low viscosity differential between the two lithologies involved, and boudinage, rather related to a high viscosity differential, are observed. Such a combination could result from a succession of two deformation events which occurred under different conditions, and thus leading to different viscosity contrasts. However, field observations instead suggest that both deformation markers developed at the same time (Ábalos et al., 2003; Girardeau and Gil Ibarguchi, 1991; Jamaa, 1988). Considering that in a dry shallow (0.5 to 1.5 GPa and up to 1100 °C) mantle, flow laws predict that dunite would have a similar viscosity than websterites and predict the websterite to be more viscous in an hydrated shallow mantle (AvéLallemant, 1978), the addition of a hydrous fluid during deformation in a dry environment or the presence of an interstitial fluid in the websterites during deformation in a hydrated environment may both bring the

viscosity contrast to a tipping point where boudinage and isoclinal folding could be developed simultaneously (AvéLallemant, 1978). Considering that the Cabo Ortegal pyroxenite originated most likely from a sub-arc mantle (Tilhac et al., 2016), both scenarios are possible and not mutually exclusive.

The CPO maximum points of pyroxenes and olivine may differ significantly from that of amphibole in certain samples, thus suggesting that amphibole recorded a different deformation episode as illustrated by sample CO-101-C (Fig. 6). Cpx clearly exhibits a S-type fabric while amphibole shows point maxima fitting both the foliation and lineation reference frames. Sample CO-101-C is from an area affected by sheath folds, which suggests that amphibole was still recording plastic deformation during their development which is subsequent to the high-temperature event recorded by the pyroxenes and olivine. However, it is difficult to know whether the deformation regime recorded by the amphiboles is the continuation of the high-temperature one or a different one.

It has been suggested by several authors that some of the high-pressure allochthonous units of the Cabo Ortegal Complex originated in an arc region (Albert et al., 2014; Arenas et al., 2014; Ordóñez Casado et al., 1996) and that their exhumation and emplacement were achieved following their introduction into a subduction return flow and an orogenic episode. Tilhac et al. (2016) confirmed the arc-related origin for the Cabo Ortegal pyroxenites and suggested that their introduction into the subduction channel was the result of delamination of the relatively dense pyroxenite-rich domain from a harzburgite sub-arc mantle. The relatively low-stress, high-temperature and potentially hydrous environment, as suggested by our data on cpx and olivine fabrics is consistent with such a scenario where deformation of the Cabo Ortegal pyroxenites occurred in a supra-subduction/arc-root environment.

Considering the origin of the amphibole, in agreement with petrological constraints, our EBSD data support the coexistence of syn- and post-kinematic amphibole. Lack of initial chemical equilibrium between cpx and amphibole from a Sr–Nd isotopes point of view suggests percolation of a hydrous fluid during amphibole growth but cannot rule out the possibility of a magmatic origin for the amphibole (Tilhac, 2017; Tilhac et al., 2016). However, the textural relationship of amphibole and cpx as well as the volumetric dominance of undeformed amphibole suggest that a metamorphic origin for the amphibole is more likely. The homogeneity of the amphibole fabrics and the likely low-stress environment in which the deformation occurred (the stress being still probably greater than the stress from the environment where the high-temperature deformation took place) are further indicators that the deformation was rather limited after the amphibole stability field was reached. The frequent similarity of the fabrics maximum points associated with the high temperature and low temperature events may be explained by two scenarios that are not mutually exclusive: (1) the deformation was continuous and in an almost spatially constant stress field; (2) a re-orientation of the structure occurred thank to late mylonites that would be difficult to observe on the field. Nonetheless, we conclude that petrological, geochemical and microstructural evidence is consistent with the introduction of a relatively competent, pyroxenite-rich mantle domain within a relatively softer subduction channel.

6. Conclusions

We performed EBSD analysis in order to better constrain the deformation style, metamorphic conditions and history of the Cabo Ortegal pyroxenites.

Pyroxenes and olivine reveal deformation at temperatures greater than 1000 °C under conditions that are consistent with a mantle wedge environment, potentially during the delamination from a sub-arc setting. Cpx preferentially deformed by subgrain rotation and dynamic recrystallization while opx was more likely to develop kink bands and recrystallize. The mineral fabrics indicate that dislocation creep was activated in response to this high-temperature deformation event. Cabo Ortegal pyroxenites did record a deformation episode at lower temperatures (from 800 to 500 °C) that is visible only in the amphibole fabrics, the pyroxenes having preserved a previous signal.

During deformation, replacive pyroxenites (*type-1* pyroxenites), due to their enclosed dunitic lenses, are likely to have localized the deformation and the deformed product may latter provide preferential pathways for fluid/melt percolation to produce *type-3* pyroxenites.

Our data and observations are consistent with a scenario in which the Cabo Ortegal pyroxenites: (1) originated in a supra-subduction context; (2) experienced a gravity- and probably mechanically-assisted delamination during which high-temperature deformation was recorded; (3) were later exhumed and shielded from further deformation thanks to their introduction within a relatively softer subduction channel and to the strong serpentinization of the harzburgitic and dunitic host.

The Cabo Ortegal Complex may therefore preserve an exceptional example of deformed and exhumed mantle wedge material, providing precious insights into a very common lithological feature in the Earth's upper mantle.

Acknowledgements

We are grateful to M. Bebbington for providing high-quality polished thin sections for EBSD measurements. We would also like to thank D. Adams, S.E.M. Gain and L. Spruženiece for their assistance during lab work. D. Mainprice is to be thanked for his help with MTex. The constructive comments of two anonymous reviewers are greatly acknowledged. This work was supported by the Australian Research Council grant for the ARC Centre of Excellence for Core to Crust Fluid Systems (CCFS), two Macquarie University International Postgraduate Scholarship (H.H. and R.T.), Macquarie postgraduate funds (H.H.), and Centre National de la Recherche Scientifique funds (UMR 5563, Géosciences Environnement Toulouse). The analytical data were obtained using instrumentation funded by DEST Systemic Infrastructure Grants, ARC LIEF, NCRIS/AuScope, industry partners and Macquarie University. This is contribution 969 from the ARC Centre of Excellence for Core to Crust Fluid Systems (http://www.ccfs.mq.edu.au) and 1152 in the GEMOC Key Centre (http://www.gemoc.mq.edu.au).

Appendix A. Supplementary material

Supplementary material related to this article can be found online at http://dx.doi.org/10.1016/j.epsl.2017.05.028.

References

Ábalos, B., Azcarrage, J., Gil Ibarguchi, J.I., Mendia, M.S., Santos Zalduegui, J.S., 1996. Flow stress, strain rate and effective viscosity evaluation in a high-pressure metamorphic nappe (Cabo Ortegal Spain). J. Metamorph. Geol. 14, 227–248.

Ábalos, B., Puelles, P., Gil Ibarguchi, J.I., 2003. Structural assemblage of high-pressure mantle and crustal rocks in a subduction channel (Cabo Ortegal, NW Spain). Tectonics 22, 1006.

Albert, R., Arenas, R., Gerdes, A., Sánchez Martínez, S., Fernández-Suárez, J., Fuenlabrada, J.M., 2014. Provenance of the Variscan Upper Allochthon (Cabo Ortegal Complex NW Iberian Massif). Gondwana Res.

Amiguet, E., Cordier, P., Raterron, P., 2010. Deformation of diopside single crystals at mantle pressure. TEM characterization of dislocation microstructures. Eur. J. Mineral. 22, 181–187.

Arenas, R., Díez Fernández, R., Sánchez Martínez, S., Gerdes, A., Fernández-Suárez, J., Albert, R., 2014. Two-stage collision: exploring the birth of Pangea in the Variscan terranes. Gondwana Res. 25, 756–763.

Arenas, R., Gil Ibarguchi, J., González Lodeiro, F., Klein, E., Martínez Catalán, J., Ortega Gironés, E., Pablo Maciá, J.d., Peinado, M., 1986. Tectonostratigraphic units in

the complexes with mafic and related rocks of the NW of the Iberian massif. Hercynica 2, 87–110.
AvéLallemant, H.G., 1978. Experimental deformation of diopside and websterite. Tectonophysics 48, 1–27.
Bachmann, F., Hielscher, R., Schaeben, H., 2010. Texture analysis with MTEX – free and open source software toolbox. Solid State Phenom. 160, 63–68.
Bachmann, F., Hielscher, R., Schaeben, H., 2011. Grain detection from 2d and 3d EBSD data—specification of the MTEX algorithm. Ultramicroscopy 111, 1720–1733.
Bascou, J., Tommasi, A., Mainprice, D., 2002. Plastic deformation and development of clinopyroxene lattice preferred orientations in eclogites. J. Struct. Geol. 24, 1357–1368.
Bunge, H.-J., 1982. Texture Analysis in Materials Science: Mathematical Methods. Elsevier.
Bystricky, M., Mackwell, S., 2001. Creep of dry clinopyroxene aggregates. J. Geophys. Res., Solid Earth 106, 13443–13454.
Carter, N.L., Ave Lallemant, H.G., 1970. High temperature flow of Dunite and Peridotite. Geol. Soc. Am. Bull. 81, 2181–2202.
Chen, S., O'Reilly, S.Y., Zhou, X., Griffin, W.L., Zhang, G., Sun, M., Feng, J., Zhang, M., 2001. Thermal and petrological structure of the lithosphere beneath Hannuoba, Sino-Korean Craton, China: evidence from xenoliths. Lithos 56, 267–301.
Dantas, C., Ceuleneer, G., Gregoire, M., Python, M., Freydier, R., Warren, J., Dick, H.J.B., 2007. Pyroxenites from the southwest Indian Ridge, 9–16°E: cumulates from incremental melt fractions produced at the top of a cold melting regime. J. Petrol. 48, 647–660.
Díaz Aspiroz, M., Lloyd, G.E., Fernández, C., 2007. Development of lattice preferred orientation in clinoamphiboles deformed under low-pressure metamorphic conditions. A SEM/EBSD study of metabasites from the Aracena metamorphic belt (SW Spain). J. Struct. Geol. 29, 629–645.
Dollinger, G., Blacic, J.D., 1975. Deformation mechanisms in experimentally and naturally deformed amphiboles. Earth Planet. Sci. Lett. 26, 409–416.
Frets, E., Tommasi, A., Garrido, C.J., Padrón-Navarta, J.A., Amri, I., Targuisti, K., 2012. Deformation processes and rheology of pyroxenites under lithospheric mantle conditions. J. Struct. Geol. 39, 138–157.
Gerya, T.V., Stöckhert, B., Perchuk, A.L., 2002. Exhumation of high-pressure metamorphic rocks in a subduction channel: a numerical simulation. Tectonics 21, 1056.
Getsinger, A.J., Hirth, G., 2014. Amphibole fabric formation during diffusion creep and the rheology of shear zones. Geology 42, 535–538.
Girardeau, J., Gil Ibarguchi, J.I., 1991. Pyroxenite-Rich Peridotites of the Cabo Ortegal complex (Northwestern Spain): evidence for large-scale upper-mantle heterogeneity. J. Petrol. 135 (154). Special Volume.
Helmstaedt, H., Anderson, O.L., Gavasci, A.T., 1972. Petrofabric studies of eclogite, spinel-Websterite, and spinel-lherzolite Xenoliths from kimberlite-bearing breccia pipes in southeastern Utah and northeastern Arizona. J. Geophys. Res. 77, 4350–4365.
Ismaïl, W.B., Mainprice, D., 1998. An olivine fabric database: an overview of upper mantle fabrics and seismic anisotropy. Tectonophysics 296, 145–157.
Jamaa, N.B., 1988. Les Peridotites de Bay-of-Islands (Terre Neuve) et de Cap Ortegal (Espagne): Approche Petro-Structurale.
Jung, H., Karato, S.-i., 2001. Water-induced fabric transitions in olivine. Science 293, 1460–1463.
Jung, H., Mo, W., Green, H.W., 2009. Upper mantle seismic anisotropy resulting from pressure-induced slip transition in olivine. Nat. Geosci. 2, 73–77.
Jung, H., Park, M., Jung, S., Lee, J., 2010. Lattice preferred orientation, water content, and seismic anisotropy of orthopyroxene. J. Earth Sci. 21, 555–568.
Kirby, S.H., Kronenberg, A.K., 1984. Deformation of clinopyroxenite: evidence for a transition in flow mechanisms and semibrittle behavior. J. Geophys. Res., Solid Earth 89, 3177–3192.
Ko, B., Jung, H., 2015. Crystal preferred orientation of an amphibole experimentally deformed by simple shear. Nat. Commun. 6.
Llana-Fúnez, S., Marcos, A., Galán, G., Fernández, F.J., 2004. Tectonic thinning of a crust slice at high pressure and high temperature by ductile-slab breakoff (Cabo Ortegal Complex, northwest Spain). Geology 32, 453.
Martínez Catalán, J.R., Arenas, R., Abati, J., Martínez, S.S., García, F.D., Suárez, J.F., Cuadra, P.G., Castiñeiras, P., Barreiro, J.G., Montes, A.D., Clavijo, E.G., Pascual, F.J.R., Andonaegui, P., Jeffries, T.E., Alcock, J.E., Fernández, R.D., Carmona, A.L., 2009. A rootless suture and the loss of the roots of a mountain chain: the Variscan belt of NW Iberia. C. R. Géosci. 341, 114–126.
Mauler, A., Bystricky, M., Kunze, K., Mackwell, S., 2000. Microstructures and lattice preferred orientations in experimentally deformed clinopyroxene aggregates. J. Struct. Geol. 22, 1633–1648.
Mercier, J.-C.C., Nicolas, A., 1975. Textures and fabrics of upper-mantle peridotites as illustrated by xenoliths from basalts. J. Petrol. 16, 454–487.
Muramoto, M., Michibayashi, K., Ando, J.-I., Kagi, H., 2011. Rheological contrast between garnet and clinopyroxene in the mantle wedge: an example from Higashi-akaishi peridotite mass SW Japan. Phys. Earth Planet. Inter. 184, 14–33.
Nicolas, A., Boudier, F., 2003. Where ophiolites come from and what they tell us. Spec. Pap., Geol. Soc. Am., 137–152.
Nicolas, A., Christensen, N.I., 1987. Formation of anisotropy in upper mantle peridotites—a review. In: Composition Structure and Dynamics of the Lithosphere-Asthenosphere System, pp. 111–123.
O'Reilly, S.Y., Griffin, W.L., 2013. Moho vs crust–mantle boundary: evolution of an idea. Tectonophysics 609, 535–546.
Ohuchi, T., Kawazoe, T., Nishihara, Y., Nishiyama, N., Irifune, T., 2011. High pressure and temperature fabric transitions in olivine and variations in upper mantle seismic anisotropy. Earth Planet. Sci. Lett. 304, 55–63.
Ordóñez-Casado, B., Gebauer, D., Schäfer, H., Gil Ibarguchi, J., Peucat, J., 1996. A single subduction event at ca. 392 Ma for the ultramafic-mafic HP/HT rocks of the Cabo Ortegal Complex. Geogaceta 20, 489–490.
Peucat, J.J., Bernard-Griffiths, J., Ibarguchi, J.I.G., Dallmeyer, R.D., Menot, R.P., Cornichet, J., De Leon, M.I.P., 1990. Geochemical and geochronological cross section of the deep Variscan crust: the Cabo Ortegal high-pressure nappe (northwestern Spain). Tectonophysics 177, 263–292.
Puelles, P., Ábalos, B., Gil Ibarguchi, J.I., 2009. Transposed high-pressure granulite fabrics (Cabo Ortegal, NW Spain): implications on the scales of deformation localization. J. Struct. Geol. 31, 776–790.
Puelles, P., Gil Ibarguchi, J.I., Beranoaguirre, A., Ábalos, B., 2012. Mantle wedge deformation recorded by high-temperature peridotite fabric superposition and hydrous retrogression (Limo massif, Cabo Ortegal, NW Spain). Int. J. Earth Sci. (Geol Rundsch) 101, 1835–1853.
Raterron, P., Doukhan, N., Jaoul, O., Doukhan, J.C., 1994. High temperature deformation of diopside IV: predominance of {110} glide above 1000 °C. Phys. Earth Planet. Inter. 82, 209–222.
Ross, J.V., Nielsen, K.C., 1978. High-temperature flow of wet polycrystalline enstatite. Tectonophysics 44, 233–261.
Skemer, P., Katayama, I., Jiang, Z., Karato, S.-i., 2005. The misorientation index: development of a new method for calculating the strength of lattice-preferred orientation. Tectonophysics 411, 157–167.
Soustelle, V., Manthilake, G., 2017. Deformation of olivine-orthopyroxene aggregates at high pressure and temperature: implications for the seismic properties of the asthenosphere. Tectonophysics 694, 385–399.
Tilhac, R., 2017. Petrology and Geochemistry of Pyroxenites from the Cabo Ortegal Complex, Spain. Macquarie University, p. 230.
Tilhac, R., Ceuleneer, G., Griffin, W.L., O'Reilly, S.Y., Pearson, N.J., Benoit, M., Henry, H., Girardeau, J., Grégoire, M., 2016. Primitive Arc magmatism and delamination: petrology and geochemistry of Pyroxenites from the Cabo Ortegal complex, Spain. J. Petrol. 57, 1921–1954.
Tilhac, R., Grégoire, M., O'Reilly, S.Y., Griffin, W.L., Henry, H., Ceuleneer, G., 2017. Source and timing of pyroxenite formation in the sub-arc mantle: case study of the Cabo Ortegal Complex, Spain. Earth Planet. Sci. Lett.
Weil, A.B., Gutiérrez-Alonso, G., Johnston, S.T., Pastor-Galán, D., 2013. Kinematic constraints on buckling a lithospheric-scale orocline along the northern margin of Gondwana: a geologic synthesis. Tectonophysics 582, 25–49.
Zhang, J., Greenii, H., Bozhilov, K., 2006. Rheology of omphacite at high temperature and pressure and significance of its lattice preferred orientations. Earth Planet. Sci. Lett. 246, 432–443.